Strong spin-orbit coupling and magnetism in (111) $(La_{0.3}Sr_{0.7})(Al_{0.65}Ta_{0.35})O_3/SrTiO_3$

V. V. Bal,[1] Z. Huang,[2,3] K. Han,[2,3] Ariando,[2,3,4] T. Venkatesan,[2,3,4,5,6] and V. Chandrasekhar[1,*]

[1]*Department of Physics, Northwestern University, Evanston, Illinois 60208, USA*

[2]*NUSNNI-Nanocore, National University of Singapore 117411, Singapore*

[3]*Department of Physics, National University of Singapore 117551, Singapore*

[4]*NUS Graduate School for Integrative Sciences and Engineering, National University of Singapore 117456, Singapore*

[5]*Department of Electrical and Computer Engineering, National University of Singapore 117576, Singapore*

[6]*Department of Material Science and Engineering, National University of Singapore 117575, Singapore*

(Received 1 February 2018; revised manuscript received 26 June 2018; published 7 August 2018)

Two-dimensional conducting interfaces in $SrTiO_3$-based heterostructures display a variety of coexisting and competing physical phenomena, which can be tuned by the application of a gate voltage. (111) oriented heterostructures have recently gained attention due to the possibility of finding exotic physics in these systems due to their hexagonal surface crystal symmetry. In this work, we use magnetoresistance to study the evolution of spin-orbit interaction and magnetism in (111) oriented $(La_{0.3}Sr_{0.7})(Al_{0.65}Ta_{0.35})O_3/SrTiO_3$. At more positive values of the gate voltage, which correspond to high carrier densities, we find that transport is multiband, and dominated by high-mobility carriers with a tendency toward weak localization. At more negative gate voltages, the carrier density is reduced, the high-mobility bands are depopulated, and weak antilocalization effects begin to dominate, indicating that spin-orbit interaction becomes stronger. At millikelvin temperatures, at gate voltages corresponding to the strong spin-orbit regime, we observe hysteresis in magnetoresistance, indicative of ferromagnetism in the system. Our results suggest that in the (111) $(La_{0.3}Sr_{0.7})(Al_{0.65}Ta_{0.35})O_3/SrTiO_3$ system, low-mobility carriers that experience strong spin-orbit interactions participate in creating magnetic order in the system.

DOI: 10.1103/PhysRevB.98.085416

I. INTRODUCTION

The two-dimensional carrier gas (2DCG) in $SrTiO_3$ (STO) -based heterostructures has been a source of great research interest since its discovery in 2004 [1], due to the variety of tunable physical phenomena it displays [2–5]. A multitude of experimental probes have revealed magnetic behavior in these systems. In particular, magnetoresistance (MR) measurements have shown signatures of the Kondo effect [2,6], anisotropic MR [7–9], and the anomalous Hall effect without hysteresis [10], as well as hysteretic MR [2,3,6,11,12], with varying temperature (T) and gate voltage (V_g) dependencies. Although there is no consensus yet, theories of magnetism rely on an understanding of the band structure to determine interactions between local moments and/or itinerant electrons. One of the important parameters affecting the band structure is the spin-orbit interaction (SOI), which has been shown to be strong in STO-based 2DCGs. This SOI, which is tunable by the application of V_g [13], can also play a more direct role in determining the ground state of the system by giving rise to various spin textures [14], which are very interesting from the point of view of applications as well as fundamental physics [15].

So far, the band structure has been widely studied in the case of (001) oriented STO-based systems. The degeneracy of the Ti $3d$ t_{2g} orbitals in (001) STO is broken near the interface, with the in-plane d_{xy} orbitals of lowest energy, while the d_{yz} and d_{zx} orbitals are higher in energy [16]. The electrons initially occupy the d_{xy} bands, but as the carrier density is increased by increasing V_g, the d_{yz} and d_{zx} bands start to become occupied [17]. In (001) LAO/STO, magnetism is believed to arise from the d_{xy} orbitals [18]. The SOI is typically seen to increase as V_g is increased, as demonstrated by MR studies in which the low-field MR goes from negative to positive as V_g is increased [13]. The band structure in the case of (111) oriented STO-based systems is very different, and it shows a hexagonal symmetry of the Ti $3d$ t_{2g} bands [19–22]. According to angle-resolved photoemission (ARPES) studies on vacuum cleaved (111) STO [20], these bands are almost degenerate at the Γ point. First-principle studies on (111) oriented perovskite heterostructures show that the trigonal crystal field and SOI can split the degeneracy of the Ti $3d$ t_{2g} manifold, and that the orbital ordering is sensitively dependent on strain [21,22]. How this complex band structure affects various properties is just beginning to be explored [23,24]. Recent transport experiments on (111) $LaAlO_3$/STO (LAO/STO) have shown surprising anisotropies related to the crystalline axes, dependent on an applied V_g [9,25–29], as well as a nonmonotonic dependence of phase-coherence time τ_ϕ and spin-orbit scattering time τ_{so} on V_g [30]. Here we report studies of the MR of $(La_{0.3}Sr_{0.7})(Al_{0.65}Ta_{0.35})O_3$ (LSAT) deposited epitaxially on (111) STO. LSAT has a 1% lattice mismatch with STO, as opposed to a 3% mismatch in the case of LAO/STO [31], which leads to a comparatively lower strain. As with the (001) LAO/STO heterostructures, we find that the SOI can be tuned by V_g. Unlike the (001) LAO/STO heterostructures [13], the SOI *increases* as V_g is tuned to more negative values. Along with this increase in SOI, at millikelvin temperatures, we see an onset of hysteresis in the MR, a signature of magnetic

*Corresponding author: v-chandrasekhar@northwestern.edu

order. This correlation suggests that SOI may play an important role in the magnetism that has been observed in STO-based heterostructures.

II. SAMPLE FABRICATION AND MEASUREMENT

We measured the MR of four Hall bars fabricated using photolithography and Ar ion milling on a single chip, with two of them aligned along the $[1\bar{1}0]$ surface crystal direction and the other two along the $[\bar{1}\bar{1}2]$ direction. The length of the Hall bars was 600 μm and the width was 100 μm. The sample had 12 monolayers of LSAT deposited on (111) oriented STO using pulsed laser deposition, at a growth partial oxygen pressure of 10^{-4} Torr [31,32]. No post growth annealing step was performed. Ti/Au was deposited on contact pads of the Hall bars, and Al wirebonds were made to allow for a four-probe measurement of transverse and longitudinal resistance. The sample was attached to a copper puck using silver paint, which allowed for the application of V_g. Measurements in field perpendicular to the sample plane were performed in an Oxford Kelvinox 300 dilution refrigerator, while measurements in field parallel to the sample plane were carried out in an Oxford Kelvinox MX100 refrigerator. Standard lock-in measurement techniques were used, with an ac frequency of 3 Hz and an ac current $\sim$100 nA. The data for all the Hall bars were qualitatively similar [33] and the trends observed were reproducible over multiple cool-downs: unlike the (111) LAO/STO devices [25], we did not observe systematic differences between Hall bars aligned along the two crystal directions. Consequently, here we show detailed data for only one Hall bar aligned along the $[\bar{1}\bar{1}2]$ direction. To maintain a uniform protocol, V_g was swept multiple times between 100 and -40 V at 4.2 K to make sure the sample was in the reversible electrostatic doping regime [34], after which the MR was measured at various values of V_g, changing V_g in steps of 20 V, going always from 100 to -40 V.

III. DATA AND ANALYSIS

Figure 1(a) shows the transverse Hall resistance R_{xy} at $T = 4.2$ K for various values of V_g. The sign of the Hall resistance is electronlike for all values of V_g in this study. At higher values of V_g, the Hall resistance is nonlinear: a knee exists in the Hall response for $V_g = 100$ V at $B_\perp \sim 2.5$ T, and moves to higher fields as V_g is decreased. The Hall response appears to be linear for $V_g \lesssim 20$ V. This transition from a nonlinear to a linear Hall effect as V_g is decreased is similar to what is observed in the case of (001) STO-based systems [17], and it has been interpreted there as a transition from multicarrier transport to single carrier transport. Based on the expected band structure from simple tight-binding approximations as well as ARPES studies [19,20], one expects two electron bands of the t_{2g} manifold to be degenerate with one effective mass, while the remaining electron band has a different effective mass. Consequently, we find that it is reasonable to describe the Hall data in terms of a two-electron band model with two different densities n_1 and n_2, and two different mobilities μ_1 and μ_2, at least for the more positive values of V_g (see the Supplemental Material [35,36]). At low magnetic fields, the resulting Hall coefficient R_H is a function of the mobilities and the densities of both bands, but in the limit of large magnetic fields, it is determined solely by the total electron density, $|R_H| \sim 1/(n_1 + n_2)$. Consequently, one should be able to qualitatively determine the dependence of the charge density by examining the behavior of the high-field Hall coefficient as a function of V_g.

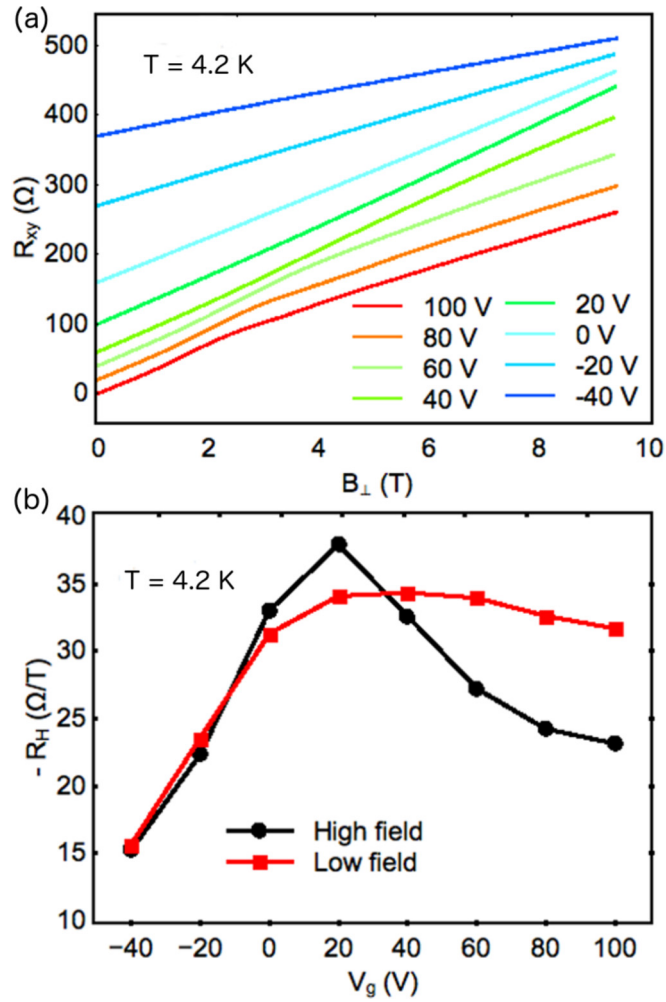

FIG. 1. (a) Hall resistance for various values of V_g at $T = 4.2$ K. Data have been antisymmetrized to remove a small contribution of longitudinal resistance due to a slight mismatch of the position of Hall probes along the length of the Hall bar. Data are also displaced along the vertical axis for clarity. (b) Low-field (red squares) and high-field (black dots) Hall slopes for data taken at 4.2 K. The low-field and high-field values correspond to values of the derivative of the Hall resistance with respect to $B_\perp$ at $B_\perp = 0$ and 9 T, respectively.

Figure 1(b) shows the low- and high-field values of $R_H = dR_{xy}/dB_\perp$ as a function of V_g. For $V_g > 20$ V, the high-field $|R_H|$ decreases with increasing V_g. Since the density of electrons increases with increasing V_g, this dependence is expected. For $V_g < 20$ V, however, the high-field $|R_H|$ decreases as V_g is reduced. This dependence is inconsistent with the presence of only electronlike bands discussed above, even if the mobilities of the electron bands are reduced with decreasing V_g. In the case of (111) LAO/STO devices, a similar dependence was observed [25], where it was ascribed to the presence of holes in addition to electrons at the interface. The presence of holelike carriers has also been recently found in (001) oriented (p-type) STO/LAO/(n-type) STO heterostructures [37]. We believe a

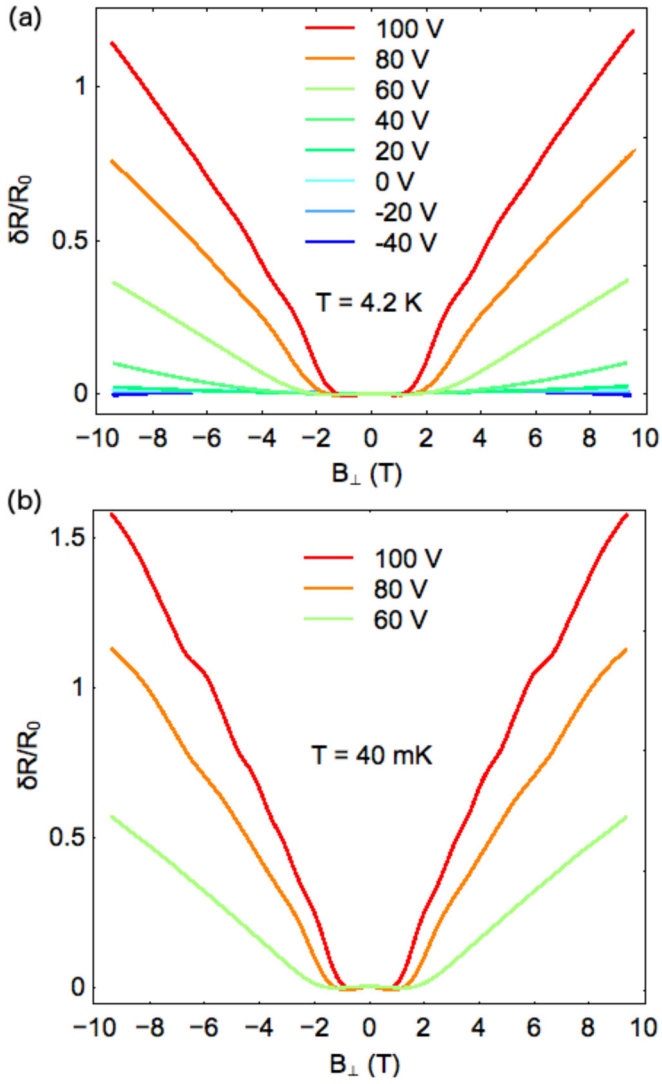

FIG. 2. (a) Differential MR at $T = 4.2$ K for various values of V_g. (b) Differential MR for $V_g = 100$, 80, and 60 V at $T = 40$ mK.

similar situation exists in these (111) LSAT/STO devices. Low-mobility holelike carriers are important at lower values of V_g, and they may be present even at higher values of V_g. The low-field R_H has a qualitatively similar (albeit weaker) dependence on V_g, and low-field and high-field R_H begin to coincide for $V_g < 20$ V, reflecting the fact that the Hall resistance is linear over the entire range of field at these gate voltages.

Evidence for multiband transport is also found in the longitudinal MR data shown in Figs. 2(a) and 2(b). For $V_g =$ 80 and 100 V, the MR is large and positive, and it shows evidence of Shubnikov–de Haas (SdH) oscillations, which are more pronounced at lower temperatures. Such oscillations are expected when $\omega_c\tau > 1$, where $\omega_c = eB_\perp/m^*$ is the cyclotron frequency, m^* is the effective mass, and τ is the scattering time. The fact that SdH oscillations are seen starting at relatively low fields ($B_\perp \sim 1.5$ T) indicates that the mobility of the carriers for large positive V_g is large. Fourier analysis of the oscillations at $V_g = 100$ V as a function of $1/B_\perp$ shows two dominant frequencies at 15 and 40 T, indicating the presence of two kinds of high-mobility carriers at this value of V_g, with carrier densities of $\sim 10^{11}$ and $10^{12}/\text{cm}^2$ (see the Supplemental Material [35]). Near zero field, one observes a negative MR, consistent with weak localization effects, discussed in more detail later. We note that the high-field MR does not saturate, as would be expected for a system with closed orbits and only electronlike carriers, but instead shows a quasilinear increase [38]. In our sample, we believe the likely causes for the quasilinear MR are some degree of compensation [38], as suggested by the Hall data, and the presence of sample inhomogeneities [39], which are unavoidable in these perovskite samples. Our present data do not allow us to distinguish between the two mechanisms.

As V_g is reduced, the overall magnitude of the MR decreases dramatically, and SdH oscillations disappear. The absence of SdH oscillations is expected, as the resistivity increases and μ decreases rapidly with decreasing V_g (see the Supplemental Material [35]). Semiclassically, for a single band system the longitudinal resistances vanishes. The MR is also expected to be very small for low-mobility carriers. We believe that the rapid decrease in the magnitude of the longitudinal MR below $V_g \sim 20$ V is associated with the concomitant depopulation of high-mobility electron bands that were occupied at higher gate voltages. Thus transport below $V_g \sim 20$ V is due to low-mobility electrons and holes. The remanent MR is small, and as we explain below, associated with quantum interference corrections to the resistance.

We now focus on the low-field MR at 4.2 K, shown in Fig. 3(a). The longitudinal MR at low fields is negative for $V_g > 20$ V and positive below this value. In LAO/STO heterostructures, the low-field MR has been associated with coherent backscattering, i.e., weak localization effects, and we believe that the origin of the low-field MR here is the same. For a two-dimensional system, in the presence of spin-dependent scattering, the weak localization contribution to the normalized differential resistance can be expressed as [40]

$$\frac{\delta R}{R_0} = \frac{R(B) - R(0)}{R(0)} = -\frac{3}{2} f(\ell_2, B) + \frac{1}{2} f(\ell_1, B), \qquad (1)$$

where the first term is the triplet Cooperon contribution, and the second term is the singlet contribution. Here $\ell_2^{-2} = \ell_\phi^{-2} + (4/3)\ell_{\text{so}}^{-2} + (2/3)\ell_s^{-2}$ and $\ell_1^{-2} = \ell_\phi^{-2} + 2\ell_s^{-2}$, where ℓ_ϕ, ℓ_{so}, and ℓ_s are the electron phase-coherence length, the spin-orbit scattering length, and the magnetic scattering length, respectively. In a quasi-two-dimensional system, the function f, written in terms of the characteristic fields $B_i = (h/2e)/(2\pi\ell_i^2)$, is given by [41]

$$f(B_i, B) = \frac{e^2 R_\square}{2\pi^2\hbar}\left[\Psi\left(\frac{1}{2} + \frac{B_i}{B}\right) - \ln\left(\frac{B_i}{B}\right)\right]. \qquad (2)$$

We note that Eqs. (1) and (2) written in this way do not involve the elastic scattering time except through the sheet resistance $R_\square$, which is a measured quantity and not a fitting parameter. There are two remaining fitting parameters, ℓ_1 and ℓ_2. It is very difficult to obtain reliable quantitative estimates for ℓ_ϕ, ℓ_{so}, and ℓ_s from fitting a single low-field MR trace to Eq. (1). The fits are sensitive to ℓ_2 and ℓ_1 only when these lengths are comparable in magnitude. To see this, consider the case when magnetic scattering is weak, so that we can ignore the terms involving ℓ_s. When $\ell_{\text{so}} \gg \ell_\phi$, the fits will depend on ℓ_ϕ, but they are insensitive to ℓ_{so}. In this case,

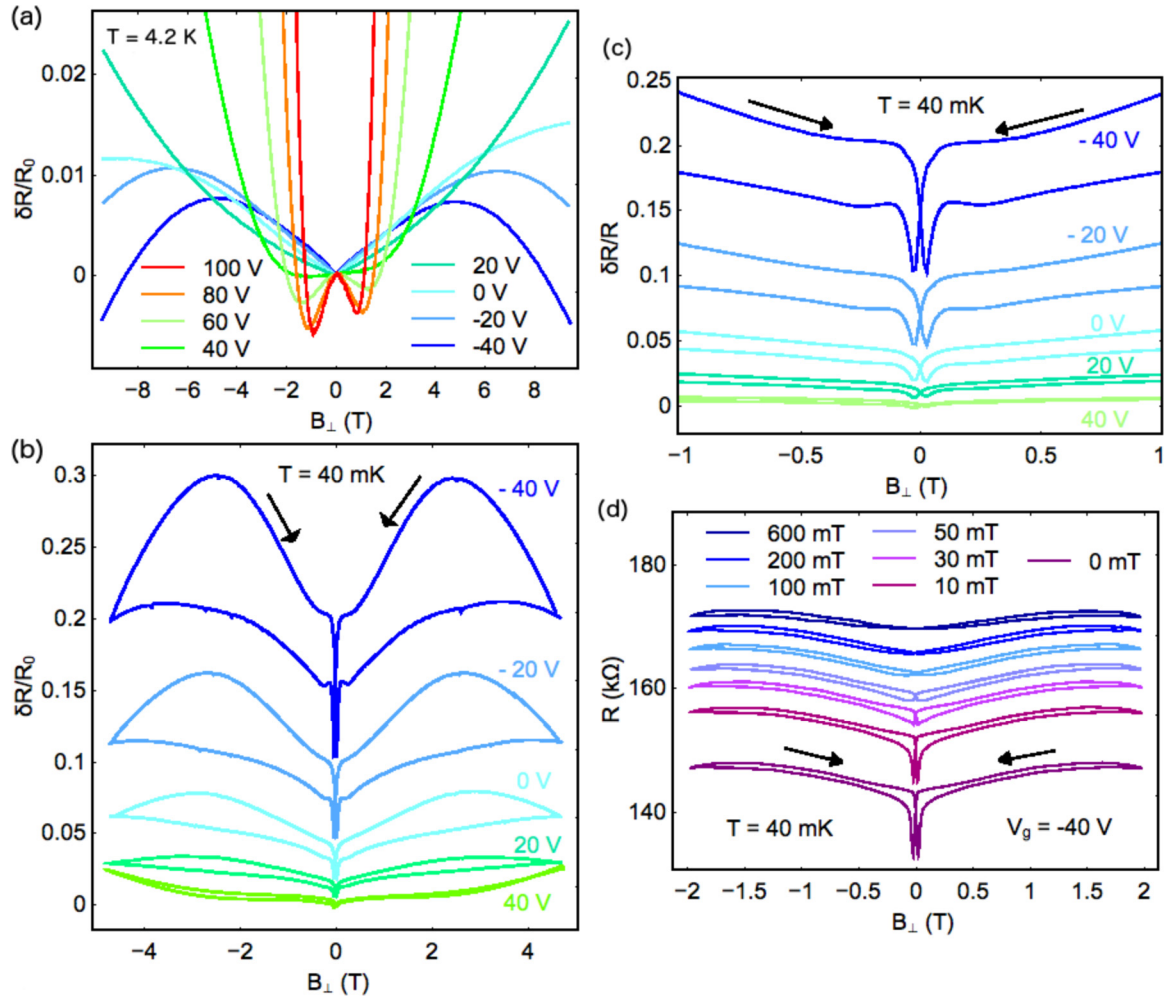

FIG. 3. (a) Differential MR at $T = 4.2$ K for various values of V_g. (b) Differential MR at $T = 40$ mK for $V_g < 60$ V. The data are shifted along the vertical axis for clarity. Arrows show the direction of the magnetic-field sweep, swept at the rate of 2.78 mT/s. (c) Same data as in (b), zoomed in to lower field values. (d) MR as a function of $B_\perp$ swept at the rate of 1.2 mT/s, measured with various values of the in-plane field held constant for $V_g = -40$ V at $T = 40$ mK.

$f(B_2, B) \sim f(B_1, B)$, and the low-field MR is negative, corresponding to weak localization. In the opposite limit, $\ell_{so} \ll \ell_\phi$, the triplet term in Eq. (1) is much smaller than the singlet term. Here one observes a low-field MR that is positive, corresponding to weak antilocalization, but the fits again depend only on ℓ_ϕ and are insensitive to ℓ_{so}. In the intermediate regime, when $\ell_{so} \sim \ell_\phi$, the MR is positive near zero field but becomes negative at higher field. It is only in this case that the fits depend on both ℓ_ϕ and ℓ_{so}. In conventional "dirty" metals such as Au, for example, one fits the low-field MR in a regime where ℓ_ϕ and ℓ_{so} are comparable, at higher temperatures, for example, using both lengths as fitting parameters, and then one fits the MR at other temperatures with only ℓ_ϕ as a fitting parameter, keeping ℓ_{so} constant to obtain ℓ_ϕ as a function of T [42].

For the present LSAT/STO devices, the situation is even more complicated, as one has contributions from the classical MR, which varies with V_g, as well as potential magnetic scattering, so obtaining reliable quantitative estimates of ℓ_ϕ and ℓ_{so} is very difficult. Nevertheless, one can draw specific conclusions about the SOI, based on the qualitative dependence of the low-field MR on V_g. We first note that ℓ_ϕ, which depends on $R_\square$, is expected to decrease in magnitude as V_g is decreased and $R_\square$ increases [13]. At $V_g \sim 100$ V then, ℓ_ϕ is comparatively large, which agrees with our earlier observation that the system at this gate voltage is relatively cleaner, showing a large classical MR that onsets at relatively low fields, and SdH oscillations. However, the low-field MR is negative, i.e., it exhibits weak localization, which from our discussion above indicates that ℓ_{so} is even larger. As V_g is reduced, ℓ_ϕ decreases, which can be inferred from the increase in the characteristic field scale, but we also observe a transition to weak antilocalization, which indicates that ℓ_{so} is decreasing even more rapidly with V_g. Indeed, the transition between negative to positive MR near zero field occurs for $V_g \leqslant 20$ V, the same value of V_g at which we see a decline in the magnitude of the large-field MR [Fig. 2(a)], which we associated earlier with the depopulation of an electron band. This suggests that the increase in SOI is related to the depopulation of electron bands as a function of V_g. The smaller SOI at large values of V_g, and hence of the associated electric field, indicates that the SOI may be primarily of the atomic type, although some studies also report a reduction in Rashba SOI with increasing V_g, related to a change in the shape of the confining potential for the 2DCG [43].

Another striking transition that occurs around the same value of V_g but at millikelvin temperatures can be seen by examining the large-field scale MR at various gate voltages, shown in Figs. 2(b) and 3(b). For $V_g \geqslant 60$ V, the MR is nonhysteretic; for $V_g \leqslant 40$ V, the MR becomes progressively more hysteretic as V_g is decreased. We can distinguish two components to this hysteresis, both of which have also been observed in LAO/STO devices [2,11,44,45]: a large background hysteresis, which is associated with the increasing glassiness of the sample with decreasing V_g, and two sharp mirror-symmetric dips at low fields [Fig. 3(c)], which we associate with the presence of long-range magnetic order in the system. Both hysteretic contributions decrease in magnitude with increasing temperature and by decreasing the sweep rate of the magnetic field (see the Supplemental Material [35]), as has also been observed in LAO/STO structures. The magnetic origin of the low-field dips can be seen by applying an in-plane magnetic field, which suppresses the low-field hysteretic dips, but not the high-field hysteresis [Fig. 3(d)]. Thus, in concert with the depopulation of the electron band and corresponding increase in spin-orbit scattering with decreasing V_g, there is an onset of magnetic order in the system, strongly suggesting that this magnetic order is related to the turn-on of SOI in the system.

IV. CONCLUSIONS

To summarize, we have studied the transverse and longitudinal MR of Hall bars fabricated on a (111) LSAT/STO sample. Our Hall data suggest that holes contribute significantly to the low carrier density regime, which is also the regime in which a strong SOI develops as we reduce V_g. At millikelvin temperatures, the carriers in these low-energy bands participate in creating ferromagnetic order, showing that SOI may play a significant role in the development of this ferromagnetic phase. We expect the SOI to be strong, since at low V_g when the phase decoherence length is shortest, the SOI length is seen to be shorter still. We believe this result gives us important insight about the band structure and interactions of (111) oriented STO-based systems. The tunable nature of the SOI also opens the possibility of manipulating the spin textures in the system electrically. We believe that these factors should provide an excellent opportunity for applications as well as fundamental research.

ACKNOWLEDGMENTS

The U.S. Department of Energy, Office of Basic Energy Sciences supported the work at Northwestern University through Grant No. DE-FG02-06ER46346. Work at NUS was supported by the MOE Tier 1 (Grants No. R-144-000-364-112 and No. R-144-000-391-114) and Singapore National Research Foundation (NRF) under the Competitive Research Programs (CRP Award No. NRF-CRP15-2015-01). This work utilized Northwestern University Micro/Nano Fabrication Facility (NUFAB), which is supported by the State of Illinois and Northwestern University.

[1] A. Ohtomo and H. Y. Hwang, A high-mobility electron gas at the $LaAlO_3/SrTiO_3$ heterointerface, Nature (London) **427**, 423 (2004).

[2] A. Brinkman *et al.*, Magnetic effects at the interface between non-magnetic oxides, Nat. Mater. **6**, 493 (2007).

[3] D. A. Dikin, M. Mehta, C. W. Bark, C. M. Folkman, C. B. Eom, and V. Chandrasekhar, Coexistence of Superconductivity and Ferromagnetism in Two Dimensions, Phys. Rev. Lett. **107**, 056802 (2011).

[4] F. Bi *et al.*, Room temperature electronically controlled ferromagnetism at the $LaAlO_3/SrTiO_3$ interface, Nat. Commun. **5**, 5019 (2014).

[5] S. Thiel, G. Hammerl, A. Schmehl, C. W. Schneider, and J. Mannhart, Tunable quasi two dimensional electron gases in oxide heterostructures, Science **313**, 1942 (2008).

[6] P. Moetakef, J. R. Williams, D. G. Ouellette, A. P. Kajdos, D. Goldhaber-Gordon, S. J. Allen, and S. Stemmer, Carrier-Controlled Ferromagnetism in $SrTiO_3$, Phys. Rev. X **2**, 021014 (2012).

[7] A. Fête, S. Gariglio, A. D. Caviglia, J.-M. Triscone, and M. Gabay, Rashba induced magnetoconductance oscillations in the $LaAlO_3/SrTiO_3$ heterostructure, Phys. Rev. B **86**, 201105(R) (2012).

[8] X. Wang, W. M. Lü, A. Annadi, Z. Q. Liu, K. Gopinadhan, S. Dhar, T. Venkatesan, and Ariando, Magnetoresistance of two-dimensional and three-dimensional electron gas in $LaAlO_3/SrTiO_3$ heterostructures: Influence of magnetic ordering, interface scattering, and dimensionality, Phys. Rev. B **84**, 075312 (2011).

[9] P. K. Rout, I. Agireen, E. Maniv, M. Goldstein, and Y. Dagan, Six fold crystalline anisotropic magnetoresistance in the (111) $LaAlO_3/SrTiO_3$ oxide interface, Phys. Rev. B **95**, 241107(R) (2017).

[10] Y. Lee, C. Clement, J. Hellerstedt, J. Kinney, L. Kinnischtzke, X. Leng, S. D. Snyder, and A. M. Goldman, Phase Diagram of Electrostatically Doped $SrTiO_3$, Phys. Rev. Lett. **106**, 136809 (2011).

[11] M. M. Mehta *et al.*, Evidence for charge-vortex duality at the $LaAlO_3/SrTiO_3$ interface, Nat. Commun. **3**, 955 (2012).

[12] A. P. Petrović *et al.*, Emergent vortices at a ferromagnetic superconducting oxide interface, New J. Phys. **16**, 103012 (2014).

[13] A. D. Caviglia, S. Gariglio, C. Cancellieri, B. Sacépé, A. Fête, N. Reyren, M. Gabay, A. F. Morpurgo, and J.-M. Triscone, Tunable Rashba Spin-Orbit Interaction at Oxide Interfaces, Phys. Rev. Lett. **105**, 236802 (2010).

[14] S. Banerjee, O. Erten, and M. Randeria, Ferromagnetic exchange, spin-orbit coupling and spiral magnetism at the $LaAlO_3/SrTiO_3$ interface, Nat. Phys. **9**, 626 (2013).

[15] A. Soumyanarayanan, N. Reyren, A. Fert, and C. Panagopoulos, Emergent phenomena induced by spin-orbit coupling at surfaces and interfaces, Nature (London) **539**, 509 (2016).

[16] A. F. Santander-Syro *et al.*, Two-dimensional electron gas with universal subbands at the surface of $SrTiO_3$, Nature (London) **469**, 189 (2011).

[17] A. Joshua, S. Pecker, J. Ruhman, E. Altman, and S. A. Ilani, Universal critical density underlying the physics of electrons at the $LaAlO_3/SrTiO_3$ interface, Nat. Commun. **3**, 1129 (2012).

[18] J.-S. Lee, Y. W. Xie, H. K. Sato, C. Bell, Y. Hikita, H. Y. Hwang and C.-C. Kao, Titanium d_{xy} ferromagnetism at the $LaAlO_3/SrTiO_3$ interface, Nat. Mater. **12**, 703 (2013).

[19] T. C. Rödel *et al.*, Orientational Tuning of the Fermi Sea of Confined Electrons at the $SrTiO_3$ (110) and (111) Surfaces, Phys. Rev. Appl. **1**, 051002 (2014).

[20] S. McKeown Walker, A. de la Torre, F. Y. Bruno, A. Tamai, T. K. Kim, M. Hoesch, M. Shi, M. S. Bahramy, P. D. C. King, and F. Baumberger, Control of a Two Dimensional Electron Gas on $SrTiO_3$ (111) by Atomic Oxygen, Phys. Rev. Lett. **113**, 177601 (2014).

[21] D. Doennig, W. E. Pickett, and R. Pentcheva, Massive Symmetry Breaking in $LaAlO_3/SrTiO_3$ (111) Quantum Wells: A Three Orbital Strongly Correlated Generalization of Graphene, Phys. Rev. Lett. **111**, 126804 (2013).

[22] D. Xiao, W. Zhu, Y. Ra, N. Nagaosa, and S. Okamoto, Interface engineering of quantum Hall effects in digital transition metal oxide heterostructures, Nat. Commun. **2**, 596 (2011).

[23] Annadi *et al.*, Anisotropic two-dimensional electron gas at the $LaAlO_3/SrTiO_3$ (110) interface, Nat. Commun. **4**, 1838 (2013).

[24] G. Herranz, F. Sánchez, N. Dix, M. Scigaj, and J. Fontcuberta, High mobility conduction at (110) and (111) $LaAlO_3/SrTiO_3$ interfaces, Sci. Rep. **2**, 758 (2012).

[25] S. Davis, V. Chandrasekhar, Z. Huang, K. Han, Ariando, and T. Venkatesan, Anisotropic multicarrier transport at the (111) $LaAlO_3/SrTiO_3$ interface, Phys. Rev. B **95**, 035127 (2017).

[26] S. K. Davis *et al.*, Electrical transport anisotropy controlled by oxygen vacancy concentration in (111) $LaAlO_3/SrTiO_3$ interface structures, Adv. Mater. Interf. **4**, 1600830 (2017).

[27] S. K. Davis *et al.*, Anisotropic superconductivity and frozen electronic states at the (111) $LaAlO_3/SrTiO_3$ interface, Phys. Rev. B **98**, 024504 (2018).

[28] S. Davis, Z. Huang, K. Han, Ariando, T. Venkatesan, and V. Chandrasekhar, Magnetoresistance in the superconducting state at the (111) $LaAlO_3/SrTiO_3$ interface, Phys. Rev. B **96**, 134502 (2017).

[29] S. Davis, Z. Huang, K. Han, Ariando, T. Venkatesan, and V. Chandrasekhar, Signatures of electronic nematicity in (111) $LaAlO_3/SrTiO_3$ interfaces, Phys. Rev. B **97**, 041408(R) (2018).

[30] P. K. Rout, E. Maniv, and Y. Dagan, Nonmonotonic Superconductivity and Spin-Orbit Interaction Across the Phase Diagram of the (111) $LaAlO_3/SrTiO_3$ Interface, Phys. Rev. Lett. **119**, 237002 (2017).

[31] Z. Huang *et al.*, The effect of polar fluctuation and lattice mismatch on carrier mobility at oxide interfaces, Nano Lett. **16**, 2307 (2016).

[32] K. Han *et al.*, Controlling Kondo-like scattering at the $SrTiO_3$ based interfaces, Sci. Rep. **6**, 25455 (2016).

[33] V. V. Bal *et al.*, Electrostatic tuning of magnetism at the conducting (111) $(La_{0.3}Sr_{0.7})(Al_{0.65}Ta_{0.35})/SrTiO_3$ interface, Appl. Phys. Lett. **111**, 081604 (2017).

[34] J. Biscaras *et al.*, Limit of the electrostatic doping in two-dimensional electron gases of $LaXO_3$ (X = Al, Ti)/$SrTiO_3$, Sci. Rep. **4**, 6788 (2014).

[35] See Supplemental Material at http://link.aps.org/supplemental/10.1103/PhysRevB.98.085416 for a description of the Hall data in terms of the two-band model, details regarding the observed Shubnikov de Haas oscillations, analysis of the MR in terms of the weak localization picture, and a more detailed description of the sample magnetism (see Refs. [46–54] from the Supplemental Material).

[36] N. W. Ashcroft and N. D. Mermin, *Solid State Physics* (Saunders College, Philadelphia, 1976).

[37] H. Lee *et al.*, Direct observation of a two-dimensional hole gas at oxide interfaces, Nat. Mater. **17**, 231 (2018).

[38] A. B. Pippard, *Magnetoresistance in Metals* (Cambridge University Press, Cambridge, 1989).

[39] M. M. Parish and P. B. Littlewood, Non-saturating magnetoresistance in heavily disordered semiconductors, Nature (London) **426**, 162 (2003).

[40] S. Hikami, A. I. Larkin, and Y. Nagaoka, Spin-orbit interaction and magnetoresistance in the two-dimensional random system, Prog. Theor. Phys. **63**, 707 (1980).

[41] P. Santhanam, Ph.D. thesis, Yale University (1985).

[42] V. Chandrasekhar, Ph.D. thesis, Yale University (1989).

[43] J. Nitta, T. Akazaki, H. Takayanagi, and T. Enoki, Gate Control of Spin-Orbit Interaction in an Inverted $|n_{0.53}Ga_{0.47}As/|n_{0.52}Al_{0.48}AS$ Heterostructure, Phys. Rev. Lett. **78**, 1335 (1997).

[44] A. Ron, E. Maniv, D. Graf, J.-H. Park, and Y. Dagan, Anomalous Magnetic Ground State in an $LaAlO_3/SrTiO_3$ Interface Probed by Transport Through Nanowires, Phys. Rev. Lett. **113**, 216801 (2014).

[45] A. Kalaboukhov, P. P. Aurino, L. Galletti, T. Bauch, F. Lombardi, D. Winkler, T. Claeson, and D. Golubev, Homogeneous Superconductivity at the $LaAlO_3/SrTiO_3$ interface probed by nanoscale transport, Phys. Rev. B **96**, 184525 (2017).

[46] A. A. Abrikosov, Quantum magnetoresistance, Phys. Rev. B **58**, 2788 (1998).

[47] H. T. He, H. C. Liu, B. K. Li, X. Guo, Z. J. Xu, M. H. Xie, and J. N. Wang, Disorder-induced linear magnetoresistance in (221) topological insulator Bi_2Se_3 films, Appl. Phys. Lett. **103**, 031606 (2013).

[48] D. Schoenberg, *Magnetic Oscillations in metals* (Cambridge University Press, Cambridge, 2009).

[49] M. Ben Shalom, A. Ron, A. Palevski, and Y. Dagan, Shubnikov–de Haas Oscillations in $SrTiO_3/LaAlO_3$ Interface, Phys. Rev. Lett. **105**, 206401 (2010).

[50] K. Han *et al.*, Electrical properties and subband occupancy at the (La, Sr)(Al, Ta)$O_3/SrTiO_3$ interface, Phys. Rev. Mater. **1**, 011601(R) (2017).

[51] G. Bergmann, Weak localization in thin films, Phys. Rep. **107**, 1 (1984).

[52] S. Wolgast *et al.*, Magnetotransport measurements of the surface states of samarium hexaboride using Corbino structures, Phys. Rev. B **92**, 115110 (2015).

[53] J. Z. Sun, L. Chen, Y. Suzuki, S. S. P. Parkin, and R. H. Koch, Thermally activated sweep-rate dependence of magnetic switching field in nanostructured current-perpendicular spin-valves, J. Magn. Magn. Mater. **247**, 237 (2002).

[54] J. A. Bert *et al.*, Direct imaging of the coexistence of ferromagnetism and superconductivity at the $LaAlO_3/SrTiO_3$ interface, Nat. Phys. **7**, 767 (2011).